

Measurement of the Thermal Diffusivity of Solids with an Improved Accuracy¹

C. D. Martinsons^{2,3}, A. P. Levick² and G. J. Edwards²

¹ Paper presented at the Fourteenth Symposium on Thermophysical Properties, June 25-30, Boulder, Colorado, U.S.A.

² Centre for Basic, Thermal and Length Metrology, National Physical Laboratory, Teddington, Middlesex, TW11 0LW, England.

³ To whom correspondence should be addressed.

ABSTRACT

A photothermal radiometry technique is being developed at the NPL with the goal of improving the accuracy of thermal diffusivity measurements. The principle is to perform a laser-induced thermal experiment while simultaneously making accurate measurements of the experimental boundary conditions. A numerical 3D heat diffusion model based on thermal transfer functions has been developed to use the measured boundary conditions. The thermal diffusivity is estimated from the experimental data by a non-linear, least-squares fitting to the model.

Experiments carried out on pure metals at about 900K demonstrate good agreement between the theoretical and experimental data and accuracies of about 1.5% for the thermal diffusivities of platinum, titanium and germanium

KEY WORDS: optical techniques, photothermal radiometry, laser, infrared, platinum, titanium, germanium, thermal diffusivity.

1. INTRODUCTION

Photothermal techniques are being developed at the NPL for the simultaneous measurement of temperature [1] and thermophysical properties such as emissivity, thermal diffusivity and thermal conductivity. This paper describes the results of recent investigations directed particularly at improving the accuracy of thermal diffusivity measurements. Well-established techniques for the determination of the thermal diffusivity of solids such as the flash technique [2,3] or thermal wave techniques [4] often rely on simplified geometries and ideal boundary conditions used *a priori* in a mathematical model. Systematic errors inevitably occur because of experimental deviations from initial assumptions [4]. In the most widely used technique, the laser flash technique, a uniform 1D excitation and a simple temporal pulse shape are assumed [2,3]. Pulsed laser beams are in essence difficult to measure and the desired characteristics are not always met. This may partly explain why the uncertainties reported for thermal diffusivity values are rarely better than a few percent, even with high purity materials.

We propose a new methodology, based on photothermal infrared radiometry [5], to measure the thermal diffusivity of materials with a better accuracy. The principle is to detect a laser-induced thermal radiance signal while simultaneously making accurate measurements of the boundary conditions of the heat conduction problem. In the case of a sufficiently large sample opaque at the pump wavelength, the only boundary conditions are the laser beam profile at the surface and the time dependence of the incident intensity.

The excitation of the sample is achieved using a periodically scanned cw laser beam. By absorption of a fraction of the incident light, a periodic temperature field is induced which in turn is responsible for a modulation of the thermal radiance emitted by the stimulated surface.

Visible and infrared optical detection are performed in the time domain to measure the modulated thermal radiance and the back-scattered laser light. The modulated thermal radiance is proportional to a local average of the induced temperature field whereas the back-scattered signal gives the time dependence of the incident laser intensity. The beam profile is accurately measured using a beam analysing device made of a scanning slit attached to the moving mirror of a Michelson interferometer. The experimental set-up is more precisely described in section 2.

The theoretical waveform of the periodic temperature field is given by a linear relationship between the thermal source term and a heat diffusion operator. Fourier analysis of the heat conduction problem shows that the latter behaves as a low-pass filter whose cut-off frequency depends on the thermal diffusivity. Section 3 presents the mathematical model used to solve this 3D time-dependent heat conduction problem.

The thermal diffusivity is estimated from the experimental data sets by a non-linear least-squares fitting to the model. The algorithm is presented in section 4.

Experimental data on platinum, titanium, germanium and copper heated to about 900K in air are presented and discussed in section 5.

2. EXPERIMENTAL SET-UP

A schematic of the photothermal set-up is shown in Fig. 1. The sample's front surface is optically excited by an argon ion laser beam delivering a maximum power of 2 W at 514.5 nm. A laser scanner, driven by a programmable function generator, is used to periodically scan the beam across the sample's surface. A CaF₂ plano-convex doublet forms an image of a fixed point of the surface on to two optical detectors. The doublet is used in 1 to 1 imaging ratio

and has a numerical aperture of about 0.1. The optical signal is the superimposition of the back-scattered laser light and the thermal radiance emitted by sample surface. A longwave-pass germanium beamsplitter is used to transmit wavelengths greater than $1.85\ \mu\text{m}$ towards an InSb infrared detector (dimensions $0.1\text{mm} \times 0.1\text{mm}$) and to reflect shorter wavelengths towards a silicon detector which has a suppressed infrared sensitivity. The infrared thermal radiance is filtered using a narrow bandwidth interference filter centred at $4.05\ \mu\text{m}$. A narrow bandwidth detection has the advantage of minimising the effect of chromatic aberrations induced by the collecting lenses.

When a square wave is used to drive the scanner, the beam is periodically deflected on and off the targeted spot, producing a chopped laser excitation. Unlike an optical chopper, the laser scanner can be operated reproducibly at very low frequencies with a short step time ($<10\ \mu\text{s}$).

After preamplification, both the back-scattered signal and the thermal radiance signal are digitised using a 16 bits A/D card. The data acquisition is triggered by a 100kHz clock signal generated by a frequency multiplier from the low-frequency signal that drives the laser scanner. This synchronous sampling allows averaging of the signal over a great number of periods without significant drift or waveform distortion. The averaging process is realised in real time by an infinite impulse response digital filter implemented with LabView. The laser scanner driving signal is usually a 10 Hz square wave and typically the sampled sets of back-scattered and thermal radiance data consist of $N = 10000$ points.

During this data acquisition, a small fraction of the excitation laser beam is sampled using a polarising beamsplitter cube and sent to a beam analysing device. In order to measure the

beam profile at the position of the sample's surface, the beamsplitter is placed at identical optical path lengths from the sample and the beam analyser.

The beam analyser (Fig. 2) is a scanning slit whose displacement is monitored by a Michelson interferometer. A large area silicon photodiode placed behind a 10 μm wide slit is mounted on a motorised translation stage together with one of the interferometer mirrors. Using a 5 mW HeNe laser source, the movement of the assembly produces highly contrasted sinusoidal interference fringes which are detected by another silicon photodiode. Each fringe corresponds to a displacement equal to half a wavelength of the HeNe laser, i.e. $\Delta x = 0.3164 \mu\text{m}$. An electronic trigger circuit generates a reference TTL signal from the fringes signal. Both the reference signal and the scanning slit signal are fed in an A/D card and a LabView program is used to acquire one sample for every 10 fringes detected, equivalent to a slit displacement of 3.164 μm . The accuracy of the beam profile measurement is assessed by fitting a Gaussian profile to the data. The uncertainty on the beam diameter is typically 0.2%.

3. MATHEMATICAL MODELING

With a laser spot of a diameter of about 2 mm and a scanning frequency greater than a few tenths of Hertz, the thermal perturbation is confined within a volume of about 1 mm^3 for most materials. Therefore, the heat conduction problem solved for a semi-infinite medium is appropriate.

Let us assume a periodically modulated laser beam incident on the surface of an opaque semi-infinite homogeneous material. The absorbed laser light is converted into heat which diffuses in the material. In the case of an chopped-like modulation, the source term of the thermal problem can be expressed as the product of a spatial term by a temporal term:

$$q(x, y, z, t) = f(x, y)\mathbf{d}(z)h(t) \quad (1)$$

where $f(x, y)$ is the 2D beam profile, \mathbf{d} is the Dirac distribution and $h(t)$ is the time dependence of the laser intensity. The temperature field $T(x, y, z, t)$ in the material is the solution of the 3D heat conduction problem defined by the following differential system [6]:

$$\nabla^2 T = \frac{1}{D} \frac{\partial T}{\partial t} \quad (2a)$$

$$T(x, y, z, t) \Big|_{t=0} = 0 \quad (2b)$$

$$K \frac{\partial T}{\partial z} \Big|_{z=0} = -q(x, y, z, t) \quad (2c)$$

$$T(x, y, z, t) \Big|_{z \rightarrow \infty} = 0 \quad (2d)$$

$$T(x, y, z, t) \Big|_{x \rightarrow \infty} = 0 \text{ and } \frac{\partial T(x, y, z, t)}{\partial x} \Big|_{x \rightarrow \infty} = 0 \quad (2e)$$

$$T(x, y, z, t) \Big|_{y \rightarrow \infty} = 0 \text{ and } \frac{\partial T(x, y, z, t)}{\partial y} \Big|_{y \rightarrow \infty} = 0 \quad (2f)$$

K and D are respectively the thermal conductivity and the thermal diffusivity of the material.

$h(t)$, a periodic function with a frequency \mathbf{g} , can be expanded in a Fourier series:

$$h(t) = \sum_{n=-\infty}^{n=+\infty} \tilde{h}_n e^{2ipn\mathbf{g}} \quad (3)$$

where \tilde{h}_n is the n -th component of the Fourier spectrum of $h(t)$. After a transient regime, a periodic regime is established in the material. The temperature field can therefore be Fourier expanded:

$$T(x, y, z, t) = \sum_{n=-\infty}^{n=+\infty} \tilde{T}_n(x, y, z) e^{2ipn\mathbf{g}} \quad (4)$$

The terms \tilde{T}_n are the components of the Fourier spectrum of $T(x, y, z, t)$. Replacing T by its

Fourier expansion in Eqs. (2) leads to a differential system for each component \tilde{T}_n :

$$\nabla^2 \tilde{T}_n = \frac{2i\mathbf{p}\mathbf{g}}{D} \tilde{T}_n \quad (5a)$$

$$K \left. \frac{\mathcal{H}\tilde{T}_n}{\mathcal{H}k} \right]_{z=0} = -f(x, y) \tilde{h}_n \quad (5b)$$

$$\tilde{T}_n(x, y, z) \Big|_{z \rightarrow \infty} = 0 \quad (5c)$$

$$\tilde{T}_n(x, y, z) \Big|_{x \rightarrow \infty} = 0 \text{ and } \left. \frac{\mathcal{H}\tilde{T}_n}{\mathcal{H}k} \right]_{x \rightarrow \infty} = 0 \quad (5d)$$

$$\tilde{T}_n(x, y, z) \Big|_{y \rightarrow \infty} = 0 \text{ and } \left. \frac{\mathcal{H}\tilde{T}_n}{\mathcal{H}y} \right]_{y \rightarrow \infty} = 0 \quad (5e)$$

Let $\tilde{v}_n(u_x, u_y, z)$ be the 2D Fourier transform of $\tilde{T}_n(x, y, z)$ with respect to x and y :

$$\tilde{v}_n(u_x, u_y, z) = \int_{-\infty-\infty}^{+\infty+\infty} \int \tilde{T}_n(x, y, z) e^{-2i\mathbf{p}(u_x x + u_y y)} dx dy \quad (6)$$

The spatial frequencies u_x and u_y form a continuum in the real space because of the unbounded

conditions (5d) and (5e) [7]. Replacing \tilde{T}_n by its Fourier decomposition leads to a 1D

differential system for \tilde{v}_n as a function of the space variable z :

$$\left[(2i\mathbf{p}u_x^2) + (2i\mathbf{p}u_y^2) \right] \tilde{v}_n + \frac{d^2 \tilde{v}_n}{dz^2} = \frac{2i\mathbf{p}\mathbf{g}}{D} \tilde{v}_n \quad (7a)$$

$$K \left. \frac{d\tilde{v}_n}{dz} \right]_{z=0} = -\tilde{f}(u_x, u_y) \tilde{h}_n \quad (7b)$$

$$\tilde{v}_n(u_x, u_y, z) \Big|_{z \rightarrow \infty} = 0 \quad (7c)$$

where $\tilde{f}(u_x, u_y)$ is the 2D Fourier transform of the beam profile.

The solution of the differential system defined by Eqs. (7), expressed at $z=0$, is:

$$\tilde{v}_n(u_x, u_y, z) = \frac{\sqrt{D}}{K} \frac{\tilde{f}(u_x, u_y) \tilde{h}_n}{\sqrt{2i\mathbf{p}\mathbf{ng} + 4\mathbf{p}^2 D(u_x^2 + u_y^2)}} \quad (8)$$

Eq. (8) shows that the surface temperature in the Fourier domain is the algebraic product of the beam profile Fourier component $\tilde{f}(u_x, u_y)$ by the Fourier component of the laser intensity time dependence \tilde{h}_n and by a thermal transfer function $H_n(u_x, u_y)$ defined by:

$$H_n(u_x, u_y) = \frac{\sqrt{D}}{K} \frac{1}{\sqrt{2i\mathbf{p}\mathbf{ng} + 4\mathbf{p}^2 D(u_x^2 + u_y^2)}} \quad (9)$$

The surface temperature field in the Fourier domain can be seen as the result of a linear filter H acting on two input functions \tilde{f} and \tilde{h}_n :

$$\tilde{v}_n(u_x, u_y, z=0) = H_n(u_x, u_y) \tilde{f}(u_x, u_y) \tilde{h}_n \quad (10)$$

In the experimental set-up, a photodetector of dimensions x_d and y_d is used to detect the thermal radiance emitted by the surface in a small spectral band centred around the detection wavelength. In the limit of small laser heating, the signal $S(t)$ induced by the laser periodic heating is proportional to the periodic surface temperature, averaged on the detection zone.

The proportionality factor, which includes the local emissivity, the first derivative of the Planck function, the numerical aperture of the optics and the instrumental gain, is omitted for clarity:

$$S(t) = \frac{1}{x_d y_d} \int_{-x_d/2}^{x_d/2} \int_{-y_d/2}^{y_d/2} T(x, y, z=0, t) dx dy \quad (11)$$

$S(t)$ is also a periodic function and therefore can be expressed as a Fourier series with coefficients \tilde{S}_n . According to Eq. (11), \tilde{S}_n is given by:

$$\tilde{S}_n = \frac{1}{x_d y_d} \int_{-x_d/2}^{x_d/2} \int_{-y_d/2}^{y_d/2} \tilde{T}_n(x, y, z=0) dx dy \quad (12)$$

After replacing \tilde{T}_n by its 2D Fourier expansion and performing the double integration over x and y , Eq. (12) becomes:

$$\tilde{S}_n = \int_{-\infty}^{+\infty} \int_{-\infty}^{+\infty} \tilde{v}_n(u_x, u_y, z=0) \text{sinc}(\mathbf{p}x_d u_x) \text{sinc}(\mathbf{p}y_d u_y) du_x du_y \quad (13)$$

where $\text{sinc}(x) = \sin(x)/x$. Let us define the detector transfer function $T(u_x, u_y)$:

$$T(u_x, u_y) = \text{sinc}(\mathbf{p}x_d u_x) \text{sinc}(\mathbf{p}y_d u_y) \quad (15)$$

The Fourier components \tilde{S}_n of the periodic signal can now be expressed as:

$$\tilde{S}_n = \tilde{h}_n \int_{-\infty}^{+\infty} \int_{-\infty}^{+\infty} H_n(u_x, u_y) T(u_x, u_y) \tilde{f}(u_x, u_y) du_x du_y \quad (16)$$

Assuming a rotational symmetry of the laser beam, Eq. (16) becomes:

$$\tilde{S}_n = \tilde{h}_n \int_{-\infty}^{+\infty} \int_{-\infty}^{+\infty} H_n(u_x, u_y) T(u_x, u_y) \tilde{f}(u_x) \tilde{f}(u_y) du_x du_y \quad (17)$$

The periodic signal $S(t)$ is given by the following Fourier series:

$$S(t) = \sum_{n=-\infty}^{+\infty} \tilde{S}_n e^{2i\pi n g} \quad (18)$$

The numerical implementation of the model was done using MATLAB. The Fourier spectra \tilde{f} and \tilde{h}_n are computed using the Fast Fourier Transform algorithm (FFT) applied to the beam profile and the backscattered light data. The double integral in (17) is approximated by a double sum over the positive spatial frequencies. $S(t)$ is computed according to Eq. (18)

by inverse FFT. The computation of a set of 10000 values of $S(t)$ takes about 10 seconds on a 350 MHz PC.

3. PARAMETER ESTIMATION

Although the temperature and the photothermal signal are given by linear relationships, the model described in section 2 is not linear with respect to the thermal diffusivity. This parameter must be therefore estimated by a non-linear parameter estimation procedure aiming to fit the model to the thermal radiance data. Assuming Gaussian white noise with zero-mean and uniform variance, the least-squares technique provides minimal variance estimators [8]. In order to avoid any bias, the experimental data are not normalised. Instead, instrumental parameters (offset, gain and arbitrary time origin) are estimated together with the diffusivity in the form a four-parameter vector $\mathbf{m}^t = (D, \text{offset}, \text{gain}, \text{origin})$. The Gauss-Newton iterative algorithm is chosen to perform the minimisation of the least-squares cost function. In this technique, the first partial derivatives of the model with respect to the parameters are needed to compute the $N \times 4$ Jacobian matrix G of the problem:

$$G_{ij} = \left(\frac{\partial S(t)}{\partial m_j} \right)_{t=t_i} \quad (22)$$

The partial derivative with respect to the diffusivity is approximated by a finite-difference. Since the data depend linearly on the instrumental parameters, the computation of the corresponding partial derivatives is straightforward [8].

This parameter estimation problem is well-conditioned and the algorithm usually converges after 3 or 4 iterations when realistic initial values are used. An estimate $\hat{\mathbf{S}}^2$ of the variance of the noise is given by:

$$\hat{\mathbf{S}}^2 = \frac{1}{N-4} \sum_{i=1}^N \left(S_{exp}(t_i) - S_{theo}(t_i) \right)^2 \quad (23)$$

where $S_{exp}(t_i)$ and $S_{theo}(t_i)$ are respectively the measured and the fitted theoretical data.

The main source of error in the joint estimation of the diffusivity and the 3 other parameters is the noise in the thermal radiance data, which is essentially due to the background photon noise. The covariance matrix C_m of the estimated parameters is evaluated using the linear least-squares theory:

$$C_m = \hat{\mathbf{S}}^2 (G^T G)^{-1} \quad (24)$$

where G is evaluated using the optimal values of the parameters. The number of degrees of freedom of this type A uncertainty is $N-4$, which typically is 9996.

Because of the very good accuracy on the measurement of the beam profile, the induced uncertainties are considered to be negligible compared to the uncertainty induced by the thermal radiance noise.

4. EXPERIMENTAL RESULTS

The thermal diffusivities of platinum, germanium, titanium and copper have been measured. Each sample was placed in a tube furnace and heated in air to about 900 K. In the case of titanium and copper, an oxide layer formed on the surface. A beam diameter of about 2 mm and a scanning frequency of 10 Hz were used. The measured boundary conditions for the platinum sample are shown in Fig. 3. The laser power was set at about 100mW in order to minimise non-linear effects in the thermal radiance signal. A temperature perturbation of about 2 K was induced in the samples. To compensate for the very low corresponding infrared signal level, a large number of periods, typically 1000, were averaged according to the procedure described in section 2. The thermal radiance signal measured on platinum and the

best fit are shown in Fig. 4. Table I presents the results obtained with the set of samples.

The thermal diffusivities of platinum, titanium and germanium were measured with an accuracy of about $\pm 1.5\%$ at a confidence level of 95%. These results are in good agreement with the literature values [9]. Platinum, germanium and titanium gave excellent agreement between experimental and theoretical data. In contrast, the data collected with copper showed residual peaks after the fitting procedure. In this case, the homogeneous model for the sample is almost certainly not appropriate because of the thick black oxide layer formed at high temperature in air.

6. CONCLUSIONS

By accurately measuring the boundary conditions associated with a laser-based thermal experiment, it has been demonstrated that the thermal diffusivity of solids can be measured with an accuracy of about $\pm 1.5\%$. The results presented in this work concerned platinum, titanium, germanium and copper. Although the accuracies of the literature values are not generally as good, they agree well with our measurements. However, the data obtained with copper showed that the technique does not give very good results when the surface oxidises too much. A good validation of the technique would consist in measuring the thermal diffusivity of a very high purity sample in a controlled atmosphere as a function of temperature.

Using the linear system theory, it is theoretically possible to perform a real-time estimation of the thermal diffusivity by adaptive filtering. Such a filter could be implemented on a digital electronic circuit allowing the thermal diffusivity to be estimated 'on-line'.

REFERENCES

- [1] G.J. Edwards and A.P. Levick, *Proceeding of the 7th International Symposium on Temperature and Thermal Measurements in Industry and Science TEMPMEKO'99* (Imeko/Nmi Van Swinden Laboratorium, Delft, 1999) p 619
- [2] W.J. Parker, R.J. Jenkins, C.P. Butler and G.L. Abbott, *J. Appl. Phys.* **32** (9): 1679 (1961)
- [3] B. Remy, D. Maillet and S. André, *Int. J. Thermophysics* **19** (3): 951 (1998)
- [4] H.G. Walther and T. Kitzing, *J. Appl. Phys.* **84** (3): 1163 (1998)
- [5] P.E. Nordal, S.O. Kanstad, *Phys. Scr* **20**: 659 (1979)
- [6] H.S. Carslaw and J.C. Jaeger, *Conduction of Heat in Solids*, 2nd Ed. (Oxford University Press, Oxford, 1959)
- [7] M.N. Özisik, *Heat Conduction*, 2nd Ed. (Wiley, New York, 1993)
- [8] J.V. Beck and K.J. Arnold, *Parameter Estimation in Engineering and Science* (Wiley, New York, 1977)
- [9] Y.S. Touloukian, R.K. Kirby, R.E. Taylor and T.Y.R. Lee, *Thermophysical Properties of Matter* (IFI/Plenum, New York, 1972), Vol.10

Fig. 1 Photothermal radiometry set-up

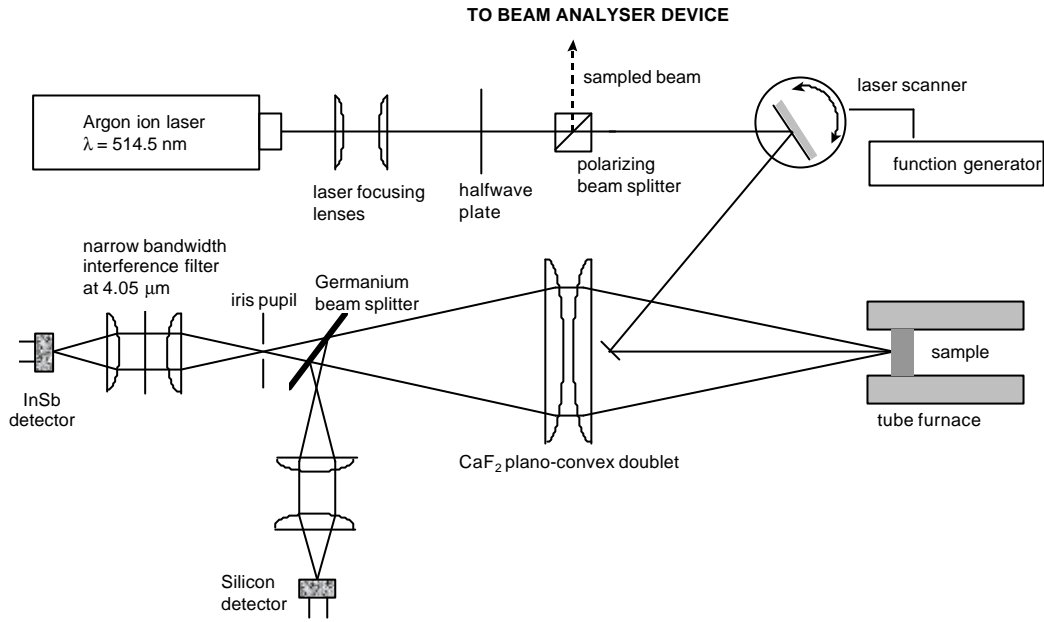


Fig. 2. Beam analyser device

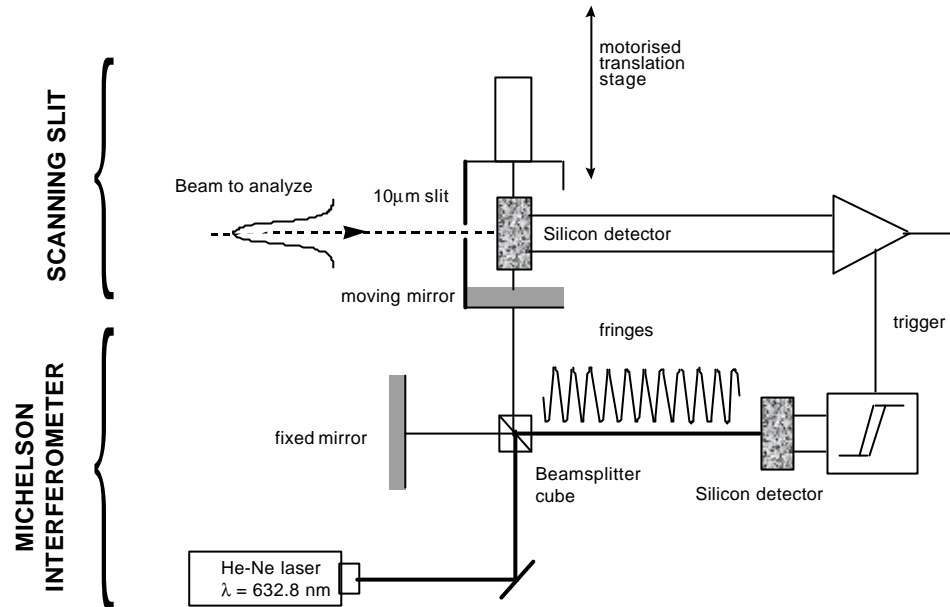


Fig. 3. Boundary conditions used for the analysis of platinum. (a) Beam profile. (b) Laser intensity time dependence. The smaller graphs shows the finite rise time of the laser excitation (~ 0.2 ms).

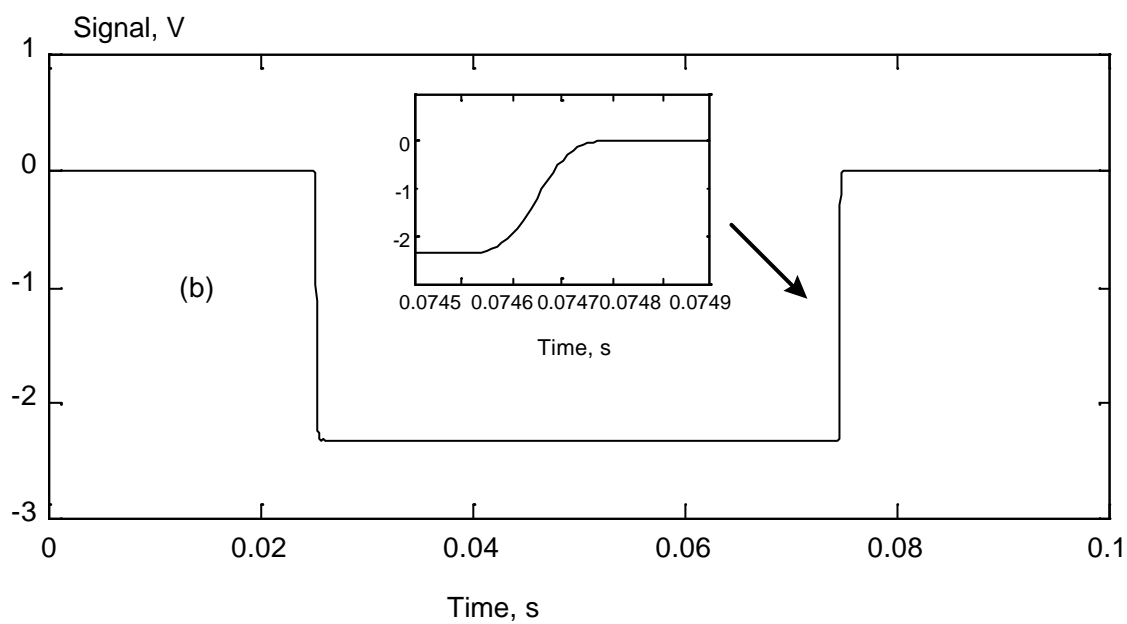
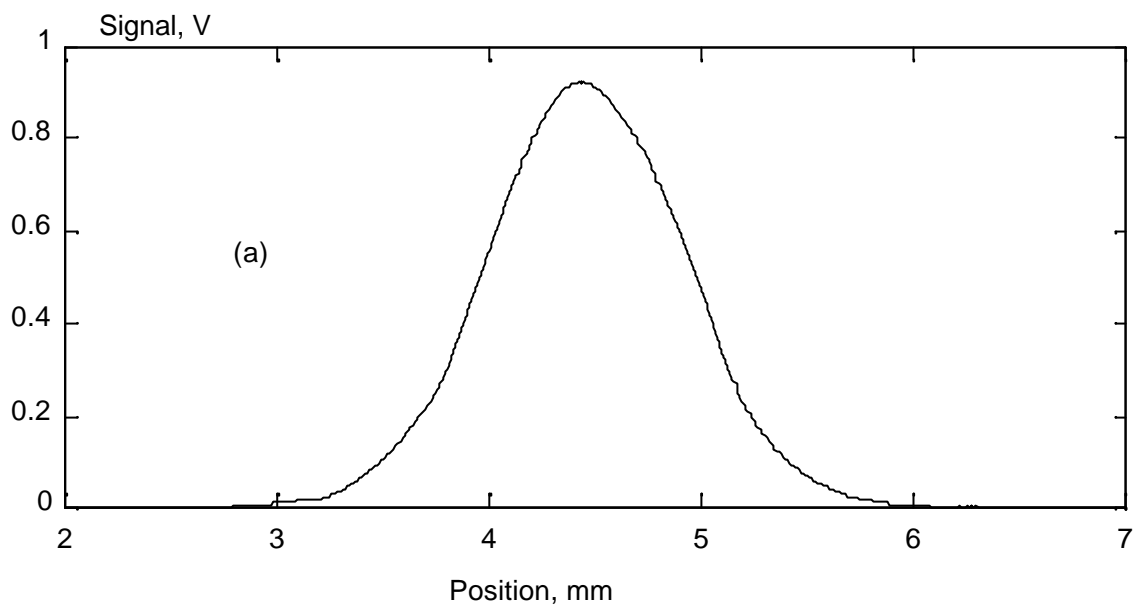


Fig. 4. thermal radiance signal measured on platinum. (a) Experimental data (noisy signal) and best fit (continuous line). (b) Data residuals after fitting.

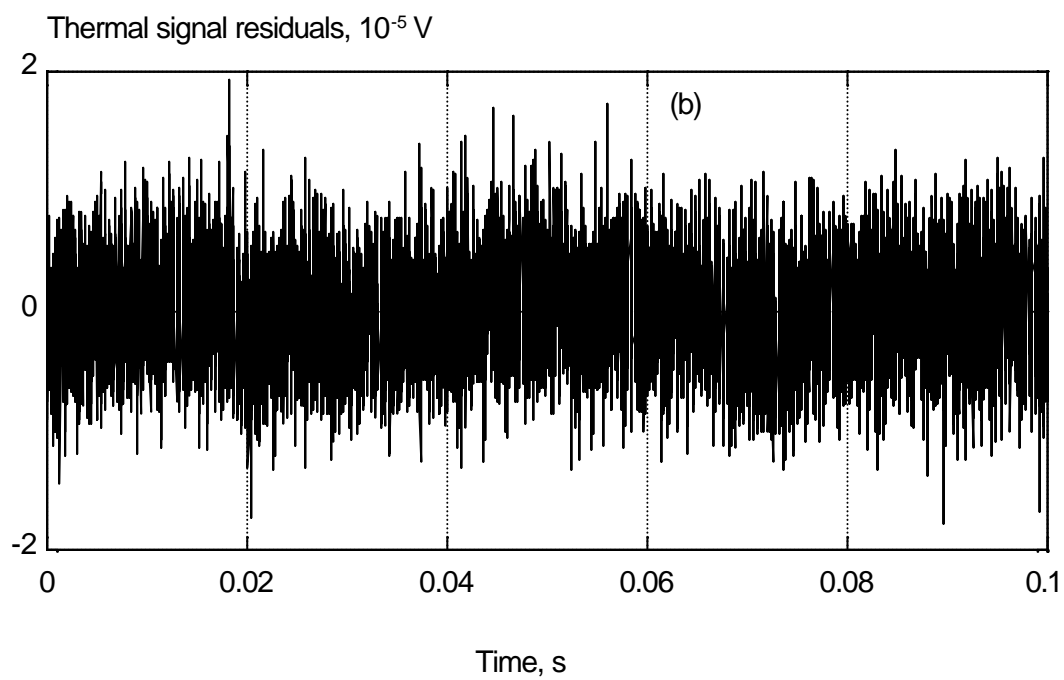
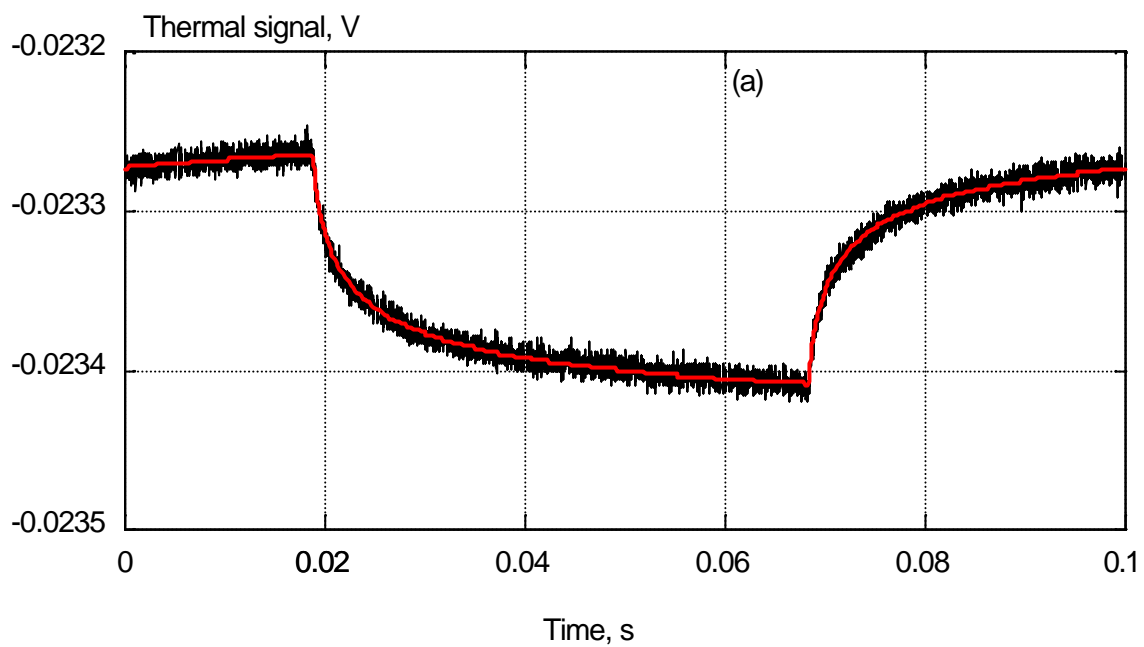


Table I. Experimental results on the thermal diffusivity of pure metals

material	purity	T	surface state	this work	literature [9]
				<ul style="list-style-type: none"> • thermal diffusivity • standard deviation • 95% conf. interval 	<ul style="list-style-type: none"> • thermal diffusivity • accuracy • conf. interval
	(%)	(K)		(m ² s ⁻¹)	(m ² s ⁻¹)
platinum	99.99	900	polished	$D = 2.56 \cdot 10^{-5}$	$D = 2.46 \cdot 10^{-5}$
			no oxide layer	$\sigma = 2 \cdot 10^{-7}$ $[2.52 ; 2.60] \cdot 10^{-5}$	$\pm 8 \%$ $[2.3 ; 2.7] \cdot 10^{-5}$
titanium	99.6	800	polished	$D = 6.43 \cdot 10^{-6}$	$D = 6.99 \cdot 10^{-6}$
			transparent oxide layer	$\sigma = 4 \cdot 10^{-8}$ $[6.35 ; 6.51] \cdot 10^{-6}$	$\pm 10 \%$ $[6.3 ; 7.7] \cdot 10^{-5}$
germanium	99.999	900	unpolished	$D = 8.70 \cdot 10^{-6}$	$D = 9.00 \cdot 10^{-6}$
			no oxide layer	$\sigma = 7 \cdot 10^{-8}$ $[8.56 ; 8.84] \cdot 10^{-6}$	$\pm 13 \%$ $[7.8 ; 10.2] \cdot 10^{-6}$
copper	unknown	900	polished	$D = 8.9 \cdot 10^{-5}$	$D = 9.35 \cdot 10^{-5}$
			black oxide layer	$\sigma = 2 \cdot 10^{-6}$ $[8.5 ; 9.3] \cdot 10^{-5}$	$\pm 6 \%$ $[8.8 ; 9.9] \cdot 10^{-5}$

